Converting Lamb modes into shear horizontal waves using a resonance-based metamaterial

Tian, Yiran, Shen, Yanfeng, Qin, Xianggui

Yiran Tian, Yanfeng Shen, Xianggui Qin, "Converting Lamb modes into shear horizontal waves using a resonance-based metamaterial," Proc. SPIE 11593, Health Monitoring of Structural and Biological Systems XV, 115930I (22 March 2021); doi: 10.1117/12.2582306

SPIE.

Event: SPIE Smart Structures + Nondestructive Evaluation, 2021, Online Only

Converting Lamb modes into shear horizontal waves using a resonance-based metamaterial

Yiran Tian[a], Yanfeng Shen[*a,b], Xianggui Qin[c]
[a]University of Michigan-Shanghai Jiao Tong University Joint Institute, Shanghai Jiao Tong University, Shanghai, 200240, China; [b]Shanghai Key Laboratory for Digital Maintenance of Buildings and Infrastructure, Shanghai,200240, China; [c]China Aviation Industry Chengdu Aircraft Industry (Group) Co., Chengdu, 610091, China

ABSTRACT

In this paper, an elastic metamaterial is presented to achieve complete conversion from Lamb modes into the fundamental shear horizontal mode. Modal analysis with Bloch-Floquet boundary condition is performed to obtain the dispersion features of the metamaterial system. By analyzing the resonant modes of the unit cell, a complete SH_0 mode generation band within the A_0 and S_0 modes bandgap can be formed in a wide frequency range. Thereafter, finite element model (FEM) harmonic analyses for an elastic metamaterial plate are carried out to explore the mode conversion efficiency. Finally, a coupled field transient dynamic FEM is constructed to acquire the response of the structure. A 30-count tone burst incident wave containing both A_0 and S_0 modes is excited to propagate into the elastic metamaterial system. The frequency-wavenumber analysis results demonstrate the achievement of the mode conversion behavior, manifested by the strong coupling between guided waves and resonant modes of the composite stubs. The proposed mode conversion behavior may possess great potential in future Structural Health Monitoring (SHM) and Nondestructive Evaluation (NDE) applications. The paper finishes with summary, concluding remarks, and suggestions for future work.

Keywords: Metamaterial, shear horizontal waves, structural health monitoring, nondestructive evaluation, mode conversion

1. INTRODUCTION

In recent years, shear horizontal (SH) ultrasonic guided waves are drawing more and more attention within Nondestructive Evaluation (NDE) and Structural Health Monitoring (SHM) communities, due to their preferred advantages over other wave types, such as the ability to propagate without mode conversion, wave dispersion, or significant amplitude attenuation[1, 2]. It is worth mentioning that the fundamental shear horizontal mode (SH_0) is non-dispersive, which contributes to simplifying the interpretation of sensing signals and improving the reliability of structural interrogation. However, pure SH waves are mostly difficult to be generated compared to other wave modes by traditional piezoelectric transducers (PZT). One way to generate them is through the electromagnetic acoustic transducers (EMATs) based on two physical phenomena, the Lorentz force and magnetostriction[3]. Vasile *et al.* theoretically and experimentally generated horizontally polarized shear waves with the combination of a periodic permanent magnet and an axially wound coil[4]. Nurmalia *et al.* explored the mode conversion of shear horizontal guided waves when impinging on smooth defects in plates. The fundamental mode (SH_0) and the first higher mode (SH_1) could be selectively generated by an EMAT[5]. Herdovics *et al.* presented a non-contact EMAT based on the Lorentz force for torsional guided-wave inspection of pipelines[6]. Recent advancements in shear-type piezoelectric wafer active sensor (PWAS) or transducer have also received increasing attention, as another approach to excite SH waves. Huan *et al.* summarized a comparative study of three types shear mode piezoelectric wafers for SH wave generation and reception[7], including the conventional in-plane poled thickness-shear (d_{15}) type, the thickness-poled thickness-shear (d_{15}) type, and the face-shear (d_{24}) type[8-11]. However, it is hard for the aforementioned transducers to selectively generate a certain guided wave mode into the host structure. In addition, each guided wave mode generally demonstrates distinctive sensitivity to different kinds of structural damage. Thus, enabling the switching of interrogating wave types between Lamb modes and SH modes from a single transducer is of great interest to the SHM and NDE community.

[*]yanfeng.shen@sjtu.edu.cn; phone +86-21-34206765 Ext. 5021; fax +86-21-34206525

Health Monitoring of Structural and Biological Systems XV, edited by Paul Fromme, Zhongqing Su, Proc. of SPIE Vol. 11593, 115930I · © 2021 SPIE
CCC code: 0277-786X/21/$21 · doi: 10.1117/12.2582306

Recently, resonance-based metamaterials with carefully designed microstructures have been investigated to provide bizarre behaviors to manipulate waves at a deep subwavelength scale[12]. Through adjusting the structural parameters of the metamaterial unit cell, phase shift of the propagating waves can be controlled, further contributing to the wave focusing, refraction, and deviation phenomena[13-15]. Kim *et al.* realized the total mode conversion between bulk P-wave and S-wave for a broad range of incidence angles by a specially designed elastic metasurface, named the transmodal metasurface[16]. Su *et al.* proposed an elastic metasurface for splitting the SV- and P-waves using full-wave finite-element simulations[17]. Noguchi *et al.* developed an acoustic metasurface design for wave motion conversion from longitudinal waves into transverse waves using topology optimization[18]. The authors' previous researches have demonstrated the wave control capability of metamaterials for achieving the selective frequency components and Lamb mode transmission[12, 19, 20]. Based on the mechanism of local resonance (LR), via exploring the vibration modes of the unit cell, the mode conversion in elastic metamaterial plates is more attractive for applications such as generating SH_0 wave mode from Lamb modes. However, to authors' best knowledge, the mode conversion behavior from fundamental plate guided Lamb waves modes (A_0 and S_0) into shear horizontal (SH_0) mode has seldom been reported.

This paper focuses on developing an aluminum-polylactic acid (PLA) composite resonance-based elastic metamaterial to achieve complete A_0 and S_0 mode conversion into SH_0 mode, owing to the formation of a frequency band within which SH_0 mode can be generated and simultaneously A_0 and S_0 modes are filtered out. In this manner, the switching of interrogating wave modes between Lamb waves and SH waves could be made possible using one transmitter, allowing to take advantage of the sensitivity of each wave mode type in the SHM and NDE procedure.

2. METAMATERIAL UNIT CELL DESIGN AND THE DISPERSION CHARACTERISTICS

This section presents the procedure and analysis of the metamaterial unit cell design. The mechanism behind the formation of a complete SH_0 mode generation frequency band and coincide A_0 and S_0 bandgap will be illustrated. To develop an in-depth understanding of such a mechanism, the resonant motions of the proposed metamaterial substructure and the pristine plate unit cell within the SH_0 mode conversion band were investigated through modal analysis.

2.1 Configuration of the metamaterial unit cell and the finite element model for numerical simulations

Figure 1(a) depicts the schematic diagram of the proposed metamaterial unit cell. It is comprised of an aluminum-PLA composite cylinder bonded on a 2-mm thickness perforated aluminum host plate. The rationale behind the choice of aluminum and PLA for the design resides in the fact that both materials are easy to obtain and fabricate. The elastic properties of the materials for the numerical modeling are listed in Table 1. It is worth mentioning that the two annular structures connecting the cylinder and the aluminum substrate are not symmetrical along the x- and y-axis, but are deflected at a certain angle, as shown in Figure 1(b). This kind of design can promise a strong coupling between the vibrational motion of the bonded composite stub along the y-direction and the aluminum substrate, contributing to the conversion of Lamb modes into SH_0 mode guided wave. Based on the LR mechanism, when the excitation frequency approaches the resonant frequency of the metamaterial microstructure, the corresponding frequency cannot propagate through the metamaterial system. Thus, a bandgap for A_0 and S_0 Lamb modes can also be established.

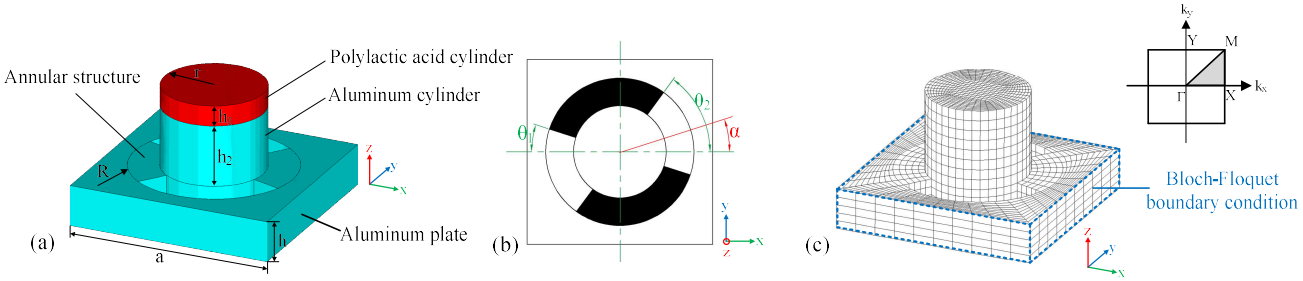

Figure 1. (a) The schematic diagram of an aluminum-PLA composite cylinder on a perforated aluminum host plate; (b) top view of the metamaterial unit cell; (c) 3D view of the finite element model and the irreducible Brillouin zone with primitive vectors.

Figure 1(c) shows the finite element model for calculating the dispersion relation by treating a unit cell with the Bloch-Floquet boundary condition. This study employed standard element codes for the computation of dispersion curves[21]. By periodic, it means that the structure is comprised of many finite-sized unit cells arranged in a regular pattern. Thus, a unit

cell with the periodic boundary condition may represent the entire metamaterial system. The standard finite element code ANSYS 15.0 package was utilized for the dispersion characterization purpose.

Table 1. Elastic properties of the materials used for the numerical simulation.

Material parameters	Elastic modulus (GPa)	Poisson's ratio	Density (kg/m^3)
Aluminum	70	0.33	2700
PLA	3.5	0.36	1250

2.2 Influence of unit cell deflection angle on the mode conversion phenomenon

To investigate the SH_0 mode-conversion effectiveness, a parametric study of the proposed metamaterial unit cell design was carried out to determine the final configuration. In this case study, the deflection angle of the structure, α, gradually increased from 0 degree to 90 degree with a step of 9 degree. Both the modal and harmonic analyses were conducted to confirm the existence of the SH_0 mode conversion band. The magnitudes of the converted SH_0 and remnant Lamb modes, owing to the limited number of the metamaterial unit cells, were also measured. Figure 2(a) and (b) exhibit the variation of SH_0 mode conversion bandwidth versus the rotational angle α. From Figure 2(a), it can be noticed that the potential mode conversion band can open for all numbers of α in modal analysis. However, from Figure 2(b) and (c), when α equals to 0 or 90 degree, forming a symmetrical structure along the midplane of the host plate, the magnitudes of the transmitted Lamb modes and converted SH_0 mode all equal to zero, i.e., the resonant power of the stub cannot be transmitted into the host plate, contributing to the transformation from the mode conversion band to a complete bandgap. As the symmetry with respect to the midplane of the plate is broken, it is remarkable that the magnitude of the converted SH_0 mode starts from zero and almost monotonically increase with the augment of α, reaching a peak at 54 degree. After that, it continues to decrease until reaching zero. In comparison with the results from modal and harmonic analyses, 18 degree is the best candidate for the metamaterial unit cell design. Considering the fact that in such a condition, the width of SH_0 mode conversion band is large enough, and the converted SH_0-mode mode amplitude dominates in the transmitted wave field with negligible Lamb wave amplitude. The geometric parameters of the optimized metamaterial unit cell design are listed in Table 2. The carefully chosen parameters ensure the satisfaction of the subwavelength requirement.

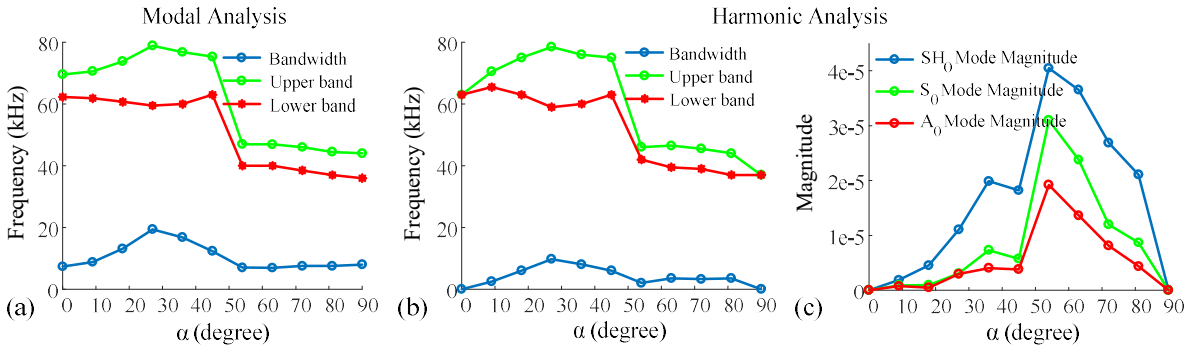

Figure 2. (a) Variation of SH_0 mode conversion bandwidth versus the rotational angle α obtained from modal analysis; (b) variation of SH_0 mode conversion bandwidth versus the rotational angle α acquired from harmonic analysis; (c) variation of magnitude of the transmitted modes versus rotational angle α from harmonic analysis.

Table 2. Geometric parameters of the optimized metamaterial unit cell.

a (mm)	h_1 (mm)	h_2 (mm)	r (mm)	R (mm)	h (mm)	α (°)	θ_1 (°)	θ_2 (°)
10	1	3	2.5	4	2	18	18	54

2.3 Coupling of wave motions between the metamaterial and the host plate

To further understand the mechanism behind the formation of such a SH_0 mode conversion band, the dispersion curves along ΓX direction within 100 kHz for the pristine plate and the metamaterial system were computed, as shown in Figure 3. Figure 3(a) exhibits the dispersion curves of a host plate unit cell, where only three fundamental wave modes, A_0, SH_0,

and S_0, are present, which means that when the excitation frequency is within this range, only three fundamental modes can propagate in the host plate. Figure 3(b) presents the dispersion curves of the metamaterial substructure, which are considerably complex due to the strong coupling and interaction between the wave motions in the plate and the composite stub. In comparison with Figure 3(a) and Figure 3(b), a directional bandgap ranging from 74-80 kHz is formed. Within the frequency range, all wave modes cannot propagate through the metamaterial substructures. Just below the directional bandgap, one may clearly observe a single branch of the dispersion curve from 62 to 74 kHz, i.e., it is a potential mode conversion and filtering band. As mentioned before, only A_0, SH_0, and S_0-mode waves can propagate through the metamaterial region into the aluminum plate. In contrast to Figure 3(a), the second band could be a potential SH_0-mode conversion band, which needs to be further investigated through a scrutiny into the vibrational motions of two substructures at the excitation frequency within the potential frequency band.

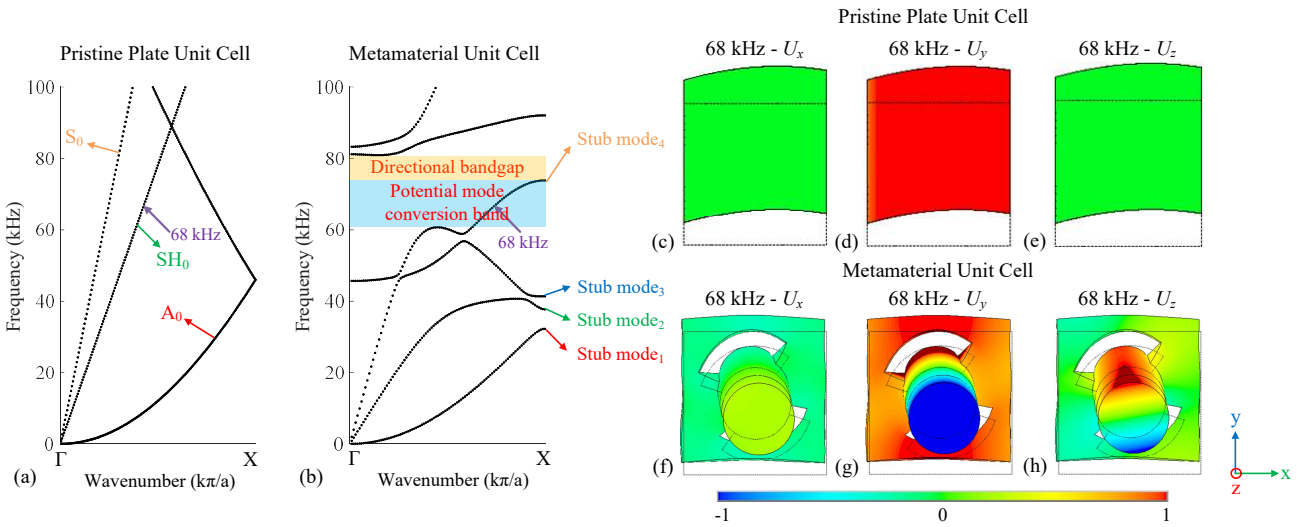

Figure 3. (a) Dispersion curves along ΓX direction within 100 kHz for the pristine host plate; (b) dispersion curves of the metamaterial unit cell along ΓX direction within the same frequency range; the resonant motions of the pristine plate and metamaterial unit cell at 68 kHz excitation frequency: (c)-(e) U_x, U_y, and U_z-displacement distributions of the pristine unit cell, and (f)-(h) U_x, U_y, and U_z-displacement distributions of the metamaterial unit cell.

Figure 3(c)-(h) display the guided wave modes of the pristine plate unit cell and the stub modes of the metamaterial unit cell at 68 kHz within the potential SH_0 mode conversion band. It can be noticed that both structures vibrate following a motion along y-direction, representing a strong coupling between the SH_0 mode in the host plate and the current stub mode in the metasurface. On the other hand, the A_0 and S_0 Lamb motions are totally decoupled from such a kind of stub mode. In other words, only the SH_0 mode is permitted to transmit through the metamaterial interface, forming an A_0 and S_0 bandgap simultaneously. Thus, the corresponding frequency range is a simultaneous SH_0 mode conversion band and Lamb modes stopping band. The displacement distributions can also support this conclusion. As can be seen from Figure 3(f) and Figure 3(h), the displacement distributions along x- and z-direction in the aluminum host plate are almost zero, which can be neglected. Whereas, the magnitude of the displacement along y-direction (Figure 3(g)) within the aluminum host plate can be clearly observed, consistent with the characteristics of SH_0 vibrational motion, as shown in Figure 3(c)-(e).

3. NUMERICAL DEMONSTRATIONS FOR THE MODE CONVERSION PHENOMENON

This section investigates the spectral response of a unit-cell-chain FEM through the harmonic analysis to verify the SH_0 mode conversion band behavior. Then, the transient dynamic modeling of the wave transmission procedure was carried out. The frequency-wavenumber analysis was adopted to identify the wave modes transmitted through the metamaterial into the host plate, to further illuminate the achievement of the SH_0 mode conversion capability.

3.1 Spectral mode conversion features

Figure 4 presents the setup for the numerical case studies. Harmonic analyses were performed to obtain the spectral responses of a pristine aluminum plate and a 10×1 unit-cell-chain model to validate the SH_0 mode conversion behavior.

As shown in Figure 4(b), a 1-kN external force sweeping from 5 kHz to 100 kHz with a step of 0.5 kHz was applied on the top surface 50-mm away from the metamaterial unit cells to simultaneously generate A_0 and S_0 modes into the structure. Two non-reflective boundaries (NRBs) were implemented at both ends of the structure to absorb the boundary reflections[22]. Periodic boundary conditions were imposed on the front and back surfaces to simulate infinitely wide structures using the finite-size stripe numerical model. Figure 5 demonstrates the frequency spectra of the A_0, SH_0, and S_0 modes decomposed from the displacement responses of two sensing points on the top and bottom surfaces of the structure.

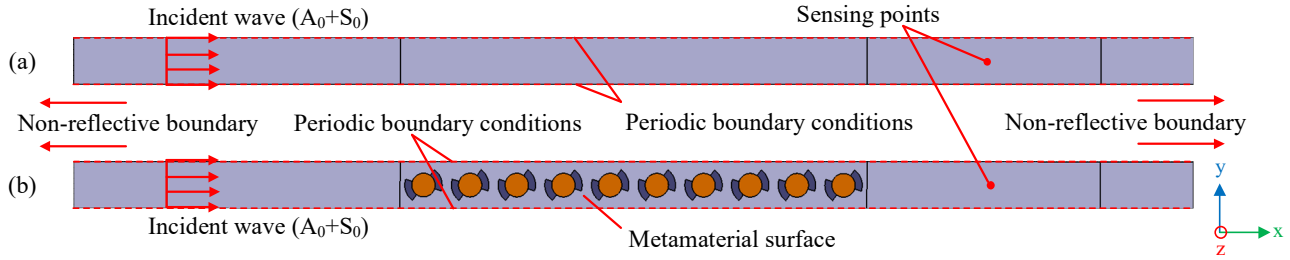

Figure 4. Numerical model with periodic boundary conditions: (a) the pristine structure; (b) the metamaterial structure.

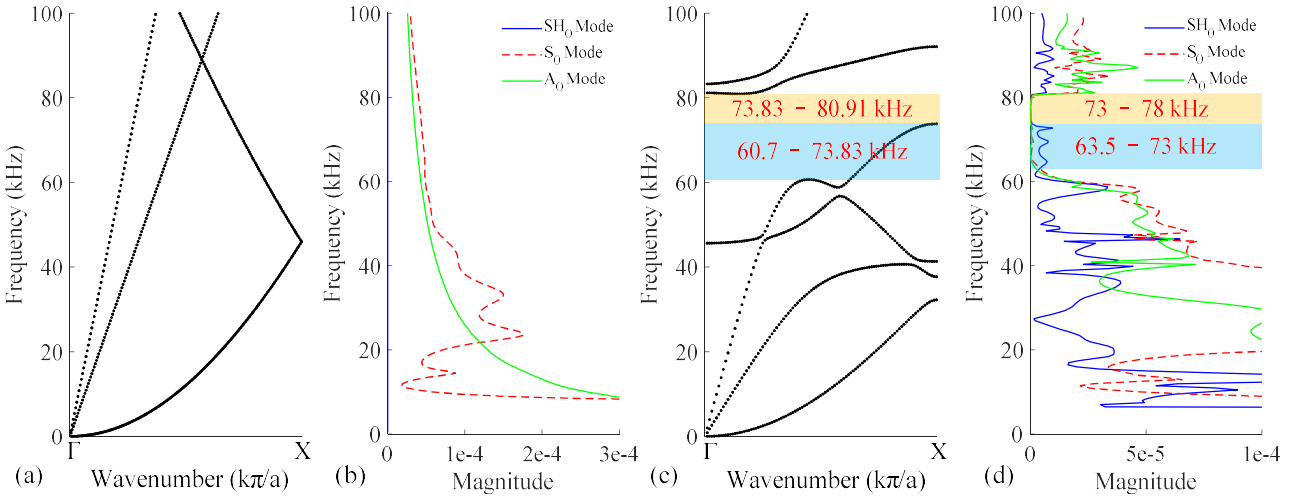

Figure 5. (a) The dispersion curves of pristine unit cell; (b) the frequency spectra of the guided wave modes at the sensing location; (c) the dispersion curves of metamaterial unit cell; (d) the frequency spectra of the guided wave modes at the sensing location.

Figure 5(c) and Figure 5(d) illustrate the comparison between the dispersion curves and frequency spectra of different wave modes in the metamaterial structural system. Two results agreed well with each other. A little deviation was caused by the limited number of the unit cells arranged along the wave propagation direction. One can clearly notice that within the directional bandgap, all the wave modes could not propagate through the metamaterial surface. Meanwhile, within the SH_0 mode conversion band, A_0 and S_0 modes were converted to SH_0 mode, i.e., A_0 and S_0 modes were filtered out and simultaneously SH_0 mode was generated by the obliquely aligned metamaterial substructures. Comparing with Figure 5(a) and Figure 5(b), the similar phenomenon cannot be observed from the pristine structure under the same circumstances. Only A_0 and S_0-mode guided waves propagated in the structure, without SH_0-mode participation.

Figure 6 shows the displacement distributions along x-, y-, and z-direction of the pristine and metamaterial model. As is well known, the in-plane displacement along x-direction of the target wave fields can effectively display the S_0 mode participation due to S_0 mode's dominant in-plane particle motion. In a similar way, the in-plane displacement along y-direction can represent SH_0 mode, and the out-of-plane displacement can denote the amplitude of A_0 mode. From Figure 6(d)-(f), at 68 kHz, within the SH_0 mode conversion band, the excited A_0 and S_0 modes could not propagate through the metamaterial region. Meanwhile, SH_0 mode was generated via mode conversion by the metamaterial unit cells and propagated into the host structure. The zoom-in area displays the vibrational motion of all the composite stubs.

Obviously, the dominant in-plane particle motion direction gradually transits from x-axis to y-axis, and the out-of-plane particle motion gradually decays until it vanishes, implying the successful conversion of SH_0 waves. However, from Figure 6(a)-(c), at the same excitation frequency, only A_0- and S_0-mode waves were involved, without any SH_0-mode wave participation. Consequently, the SH_0 mode conversion band can be verified through harmonic analysis, which agrees well with the modal analysis.

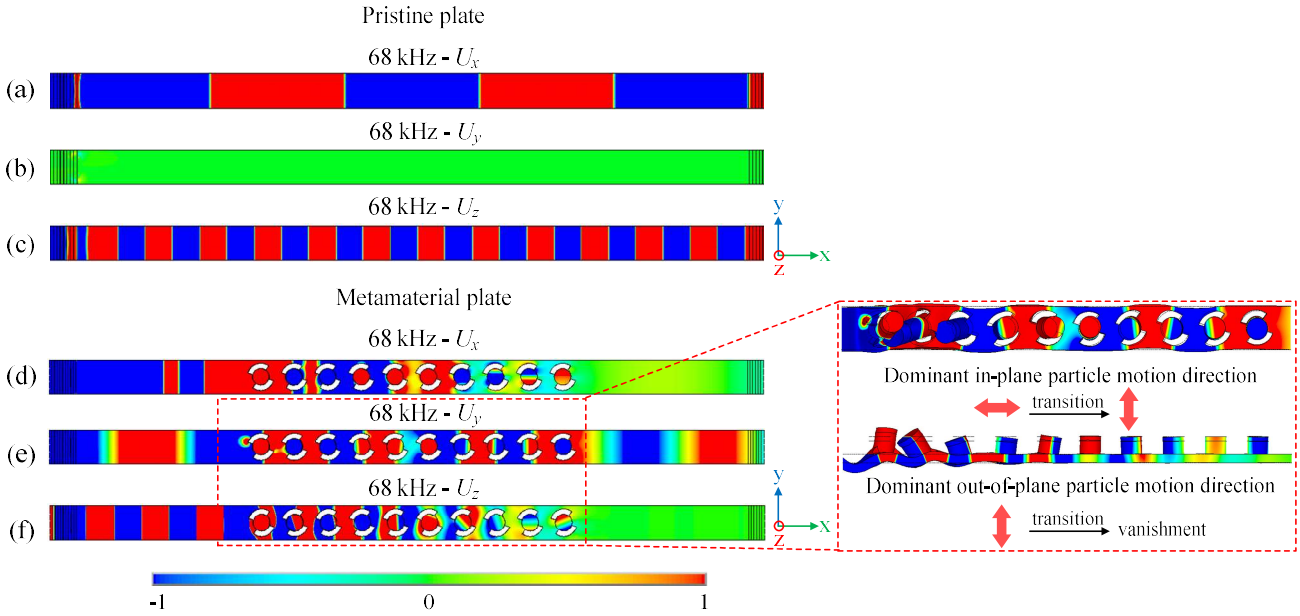

Figure 6. (a-c) The displacement distributions of the pristine structure at 68 kHz: Ux, Uy, and Uz; (d-f) the displacement distributions of the metamaterial structure at 68 kHz: Ux, Uy, and Uz. (The zoom-in area displays the resonant motions of the composite cylinders).

3.2 Transient mode conversion demonstration

Figure 7 presents the numerical model of a metamaterial chain structure for the transient dynamic analysis. Such a case of wave propagation is utilized to illustrate the SH_0 mode conversion capability. A 10 mm×10 mm×0.2 mm square PWAS was bonded on the left side of the structure 50 mm away from the left edge of metamaterial region. The data acquisition points cover a total length of 150 mm. The in-plane and out-of-plane displacements of these points on the top and bottom surfaces along the wave propagation direction was extracted to conduct the frequency-wavenumber analysis, which allows the identification of wave mode components in the transmission region. A 100 volt-peak-to-peak (vpp) 30-count Hanning-window modulated sine tone burst signal was applied on the transmitter PWAS (T-PWAS). The test frequency used in this case study was also set at 68 kHz, consistent with that in the harmonic analysis.

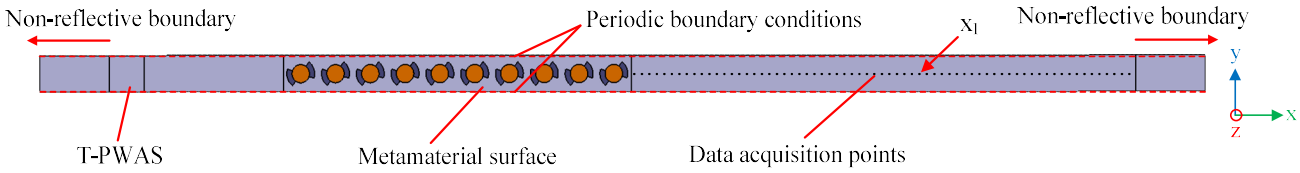

Figure 7. Numerical model setup of a metamaterial chain structure for the frequency-wavenumber analysis.

Figure 8(a) displays the representative time trace of the guided wave modes in the transmission region at x_1 location indexed in Figure 7. It can be noticed that the magnitude of the mode-converted SH_0 mode is much larger than that of A_0 and S_0 modes. Figure 8b presents the frequency-wavenumber analysis result of the transmission wave field. When the excitation frequency was 68 kHz, both A_0 and S_0 modes could not pass through the metamaterial region. However, SH_0 mode conversion behavior happened while the Lamb modes interacted with the unit cells, consistent with our conclusion of mode conversion and stopping bands. This further substantiates the mode conversion capability of the proposed metamaterial design.

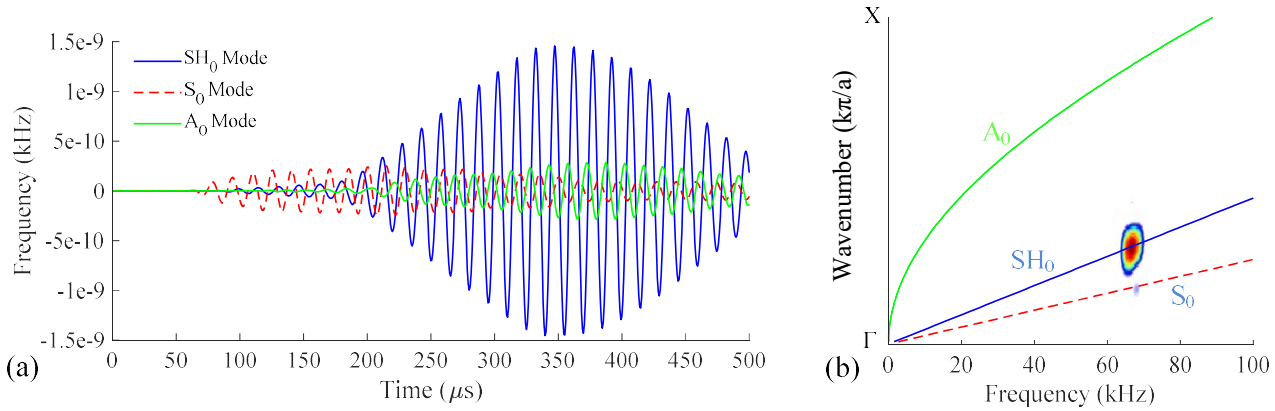

Figure 8. Transient analysis results of the wave field in the transmission region: (a) time traces of three fundamental guided wave modes at x_1 position (defined in Figure 7); (b) frequency-wavenumber domain result at 68 kHz (within the mode conversion band).

4. CONCLUDING REMARKS

In this paper, a SH_0 mode conversion control methodology using a metamaterial was put forward for potential SHM and NDE applications. A substructure was designed with an aluminum-PLA composite cylinder bonded on a perforated aluminum host plate. This kind of metamaterial can achieve a complete SH_0 mode conversion band, within which A_0 and S_0 modes are filtered out simultaneously. Through treating a unit cell with the Bloch-Floquet boundary condition, the dispersion curves of the metamaterial system along ΓX direction were numerically investigated using the modal analysis. The vibrational motions of the metamaterial substructure and the pristine unit cell at 68 kHz within the SH_0 mode conversion band were investigated. A potential mode conversion band was identified. Furthermore, the FEM harmonic analysis was conducted to obtain the spectral response of the metamaterial structure and explore the mode conversion effectiveness. It was found that within the identified frequency band, Lamb modes could not propagate through the metamaterial, while SH_0 mode was converted and transmitted. Thereafter, a coupled-field transient dynamic FEM was conducted to obtain the dynamic response of the structure. The frequency-wavenumber analysis further demonstrated the successful achievement of the SH_0 mode conversion behavior. The proposed method processes great potential in future SHM and NDE applications for selectively transmitting desired wave modes into the target area under interrogation.

For future work, active materials such as Shape Memory Alloys (SMA) and electrical-magnetic active materials should be incorporated into the design for achieving the tunable performance of the mode conversion.

5. ACKNOWLEDGEMENTS

The support from the National Nature Science Foundation of China (contract number 51605284 and 51975357) is thankfully acknowledged.

REFERENCES

[1] Kubrusly, A. C., Freitas, M. A., von der Weid, J. P., and Dixon, S., "Mode Selectivity of SH Guided Waves by Dual Excitation and Reception Applied to Mode Conversion Analysis," IEEE Trans Ultrason Ferroelectr Freq Control 65(7), 1239-1249 (2018).

[2] Kamal, A. and Giurgiutiu, V., "Shear horizontal wave excitation and reception with shear horizontal piezoelectric wafer active sensor (SH-PWAS)," Smart. Mater. Struct. 23, 085019 (2014).

[3] Remo Ribichini, F. C., Peter b. Nagy, and Peter Cawley, "Study and Comparison of Different EMAT Configurations for SH Wave Inspection," IEEE Transactions on Ultrasonics, Ferroelectrics, and Frequency Control 58(12), 2571-2581 (2011).

[4] Vasile, C. F. and Thompson, R. B., "Excitation of horizontally polarized shear elastic waves by electromagnetic transducers with periodic permanent magnets," Journal of Applied Physics 50(4), 2583-2588 (1979).

[5] Nurmalia, Nakamura, N., Ogi, H., Hirao, M., and Nakahata, K., "Mode conversion behavior of SH guided wave in a tapered plate," NDT & E International 45(1), 156-161 (2012).
[6] Herdovics, B. and Cegla, F., "Structural health monitoring using torsional guided wave electromagnetic acoustic transducers," Struct Health Monit 17(1), 24-38 (2018).
[7] Huan, Q., Chen, M., and Li, F., "A Comparative Study of Three Types Shear Mode Piezoelectric Wafers in Shear Horizontal Wave Generation and Reception," Sensors (Basel) 18, 2681 (2018).
[8] Miao, H., Huan, Q., and Li, F., "Excitation and reception of pure shear horizontal waves by using face-shear d24mode piezoelectric wafers," Smart Materials and Structures 25, 11LT01 (2016).
[9] Huan, Q., Miao, H., and Li, F., "A uniform-sensitivity omnidirectional shear-horizontal (SH) wave transducer based on a thickness poled, thickness-shear (d15) piezoelectric ring," Smart. Mater. Struct. 26, 08LT01 (2017).
[10] Miao, H., Huan, Q., Li, F., and Kang, G., "A variable-frequency bidirectional shear horizontal (SH) wave transducer based on dual face-shear (d24) piezoelectric wafers," Ultrasonics 89, 13-21 (2018).
[11] Huan, Q., Miao, H., and Li, F., "A variable-frequency structural health monitoring system based on omnidirectional shear horizontal wave piezoelectric transducers," Smart Materials and Structures 27, 025008 (2018).
[12] Tian, Y., Shen, Y., Rao, D., and Xu, W., "Metamaterial improved nonlinear ultrasonics for fatigue damage detection," Smart. Mater. Struct. 28, 075038 (2019).
[13] Zhu, H. and Semperlotti, F., "Anomalous Refraction of Acoustic Guided Waves in Solids with Geometrically Tapered Metasurfaces," Phys Rev Lett 117, 034302 (2016).
[14] Cao, L., Yang, Z., Xu, Y., and Assouar, B., "Deflecting flexural wave with high transmission by using pillared elastic metasurface," Smart Materials and Structures 27, 075051 (2018).
[15] Jin, Y., Torrent, D., Pennec, Y., Pan, Y., and Djafari-Rouhani, B., "Simultaneous control of the S0 and A0 Lamb modes by graded phononic crystal plates," Journal of Applied Physics 117, 244904 (2015).
[16] Kim, M. S., Lee, W. R., Kim, Y. Y., and Oh, J. H., "Transmodal elastic metasurface for broad angle total mode conversion," Applied Physics Letters 112, 241905 (2018).
[17] Su, X., Lu, Z., and Norris, A. N., "Elastic metasurfaces for splitting SV- and P-waves in elastic solids," Journal of Applied Physics 123, 091701 (2018).
[18] Noguchi, Y., Yamada, T., Otomori, M., Izui, K., and Nishiwaki, S., "An acoustic metasurface design for wave motion conversion of longitudinal waves to transverse waves using topology optimization," Applied Physics Letters 107, 221909 (2015).
[19] Tian, Y. and Shen, Y., "Selective guided wave mode transmission enabled by elastic metamaterials," J. Sound Vib. 485, 115566 (2020).
[20] Y. Tian and Y. Shen, "Selective Lamb Mode Transmission Enabled by Local Resonance Based Ultrasonic Metamaterial," in Proceedings of the ASME 2019 International Mechanical Engineering Congress and Exposition. Volume 11: Acoustics, Vibration, and Phononics, Salt Lake City, Utah, USA, 2019, vol. V011T01A005.
[21] M. Åberg, a. P. G., "The usage of standard finite element codes for computation of dispersion relations in materials with periodic microstructure," The Journal of the Acoustical Society of America 102(4), 2007-2013 (1997).
[22] Shen, Y. and Giurgiutiu, V., "Effective non-reflective boundary for Lamb waves: Theory, finite element implementation, and applications," Wave Motion 58, 22-41 (2015).